Optimized Measurement Timing for In-Space Thrust Inference

Oliver Jia-Richards*
University of Michigan, Ann Arbor, Michigan 48109

I. Introduction

Direct in-space thrust estimation uses measurements of a spacecraft's position or attitude over time in order to infer the thrust output of the propulsion system. Such techniques are valuable both for technology development, to determine if the thrust output matches model or laboratory predictions, as well as in-space thruster calibration and health monitoring. Of particular interest is the ability to perform direct in-space thrust estimation for low-thrust—typically electric—propulsion systems where the spacecraft's orbit or attitude will change slowly relative to the more impulsive maneuvers for a high-thrust—typically chemical—propulsion system. The Space Electric Rocket Test II (SERT II) mission provides the first instance of direct in-space thrust estimation based on using the propulsion system to perform orbital maneuvers for an electric propulsion system. A component of the thrust vector for the SERT II propulsion system was aligned with the along-track direction in order to raise or lower the spacecraft's orbit. By analyzing the change in orbit radius, the propulsive acceleration was estimated using simple analytical approximations, and then compared to thrust estimates from indirect approaches and an onboard accelerometer [1]. Recent technology demonstrations of electric propulsion systems for small spacecraft continue to leverage this analytical approximation approach [2, 3].

While purely-analytical approaches based on changes in the spacecraft's radial position provide a simple pathway to direct in-space thrust estimation from orbital maneuvers for low-thrust propulsion systems, they can be improved upon. One particular avenue for improvement is in the measurements processed to estimate the thrust magnitude. For an along-track acceleration applied to a spacecraft in a near-circular orbit, the change in radial position provides less information than the change in along-track position; the sensitivity of the radial position with respect to the acceleration magnitude is linear in time while the sensitivity of the along-track position is quadratic in time [4]. Therefore, by only considering the change in radial position, the analytical approaches leave a considerable amount of information unused. However, radial position is an absolute measurement in an Earth-fixed frame while along-track position is a relative measurement with respect to a reference trajectory. While the simple analytical approximations based on changes in the spacecraft's radial position require no reference trajectory, the incorporation of deviations in along-track position into the thrust estimation process requires the use of a numerically-simulated reference trajectory.

Numerical methods that leverage the full position of the spacecraft have typically been focused on maneuver detection and characterization for uncooperative spacecraft rather than direct in-space thrust estimation for cooperative spacecraft,

*Assistant Professor, Department of Aerospace Engineering, oliverjr@umich.edu, AIAA Member.
Presented as Paper 2024-2071 at the AIAA SciTech 2024 Forum, Orlando, FL, USA, 08–12 January 2024.

though many approaches are applicable to both problems. Maneuver detection can consist of monitoring the divergence of the measurement residuals for unmodeled maneuvers [5–7], comparing the predicted state between a filter and a smoother [8], or analyzing differences between two-line-element data and a predicted state [9, 10]. After a maneuver has been detected, it can be characterized through an adaptive variable-state dimension filter with covariance inflation [5] or through a least-squares fit of possible maneuvers to the observed measurements [7]. Multiple model approaches, where multiple filters that include or exclude potential maneuvers are run in parallel, can also be used to detect and characterize maneuvers [11, 12]. The incorporation of mission-specific information can improve transitioning between the different models by considering the probability of a spacecraft performing a maneuver based on the spacecraft state and assumed mission (e.g., station keeping for geostationary satellites) [12].

Alternative approaches utilize different assumptions regarding the maneuver optimality or functional form to improve the detection and characterization process. Optimal control distance metrics enable improved correlation between object observations and inherently detect and characterize the maneuver if the spacecraft is assumed to perform maneuvers in an energy-optimal manner [13–15]. Filter-based approaches represent an unknown maneuver using a finite Fourier series [16] or polynomial approximation [17] and represent the unknown function coefficients as state variables. Such approaches enable the determination of a continuous thrust maneuver that best represents the observed changes in spacecraft state based on the assumed functional form. The primary goal is usually to maintain tracking of an uncooperative spacecraft with the characterization of the maneuver as a valuable byproduct. For direct in-space thrust estimation the priorities are typically reversed. Continuous tracking of the spacecraft is assumed, and the primary goal is to estimate the propulsion system thrust or acceleration. The functional form of the thrust—at least over time scales short relative to potential performance degradation of the system—is also typically known, which enables more precise characterization of the propulsive acceleration than methods that assume arbitrary functional forms.

Recent developments on numerical methods for direct in-space thrust estimation with cooperative spacecraft have examined the use of least-squares batch filters [18] as well as the ensemble Kalman update [19], and the ensemble Kalman update approach has since been demonstrated on flight data for an iodine electric propulsion system [20]. While these numerical approaches enable direct in-space thrust estimation, the use of these numerical methods for optimization of the thrust estimation process is intractable. In particular, optimization of the maneuver timing, measurement timing, thrust vector direction, or other parameters in order to minimize the posterior uncertainty in the propulsion system thrust output is technically possible, but would come at great computational expense due to the need for repeated high-fidelity simulation of the spacecraft trajectory at each parameter setting. As such, there has been a push back towards more analytical approaches that analytically approximate the relationship between a piecewise-constant representation of the propulsive acceleration magnitude and measurements of the spacecraft's position with a linear measurement model [4].

The contribution of this work is to consider the problem of direct in-space thrust estimation with cooperative spacecraft, but from the perspective of optimizing the estimation process. Specifically, this work leverages the derived

linear measurement model from Ref. [4] in order to optimize the measurement timing for direct in-space thrust estimation with low-thrust maneuvers where each measurement is assumed to provide the full three-axis position of the spacecraft at a given instance in time. This problem is similar to that of sensor tasking in space situational awareness, where limited sensor resources need to be optimally scheduled in order to maintain precise tracking of a collection of spacecraft or other space objects [21–23]. However, for the direct in-space thrust estimation problem, only a single spacecraft is considered, its planned maneuver sequence is known, and continuous tracking of the spacecraft is assumed which provides additional information that can be leveraged in the optimization. Therefore, the focus of this work is not on scheduling sensor resources in order to minimize uncertainty in spacecraft trajectories for tracking purposes, but rather on scheduling limited sensor resources, either from a single sensor or multiple sensors, in order to minimize uncertainty in the propulsion system thrust output.

The results of this work provide a methodology for distributing a fixed number of measurement times in a way that will minimize the posterior variance in the propulsive acceleration magnitude. The propulsive acceleration is assumed to act in the along-track direction, such that the corresponding orbital maneuver is to raise or lower the orbital radius, and can be represented as a piecewise-constant profile. An uncertain atmospheric drag acceleration is also considered and is assumed to be spatially and temporally constant such that the estimation results effectively return the average atmospheric drag acceleration throughout the maneuver. The primary benefit of this work is for data-limited scenarios or scenarios with finite sensor resources. In both cases, the number of measurements may be constrained such that the ability to optimize the timing of the measurements becomes a valuable technique.

II. Approach

The overall problem considered in this work is the inference of the initial position and velocity of a spacecraft as well as the average atmospheric drag and propulsive accelerations based on measurements of the spacecraft's position over time. It is assumed here that the spacecraft is in a near-circular orbit around Earth, and that both the drag and propulsive acceleration vectors are aligned with the along-track direction, representative of an orbit-raising or orbit-lowering maneuver. Additionally, the propulsive acceleration is assumed to be represented by an n-segment piecewise-constant function. As such, the parameters of inference are

$$\boldsymbol{\phi} = \begin{bmatrix} \Delta r_0 & \Delta s_0 & \Delta v_{r,0} & \Delta v_{s,0} & a_d & a_1 & \dots & a_n \end{bmatrix}^T \tag{1}$$

where Δr_0, Δs_0, $\Delta v_{r,0}$, and $\Delta v_{s,0}$ represent deviations in the spacecraft's initial radial, r, and along-track, s, position and velocity relative to a known reference state, a_d is the average drag acceleration, and $a_1, \dots, a_n$ represent the acceleration magnitudes for each segment of the n-segment piecewise-constant representation of the propulsive acceleration. Deviations in position and velocity in the cross-track direction are neglected, as their sensitivities to an along-track

acceleration are zero. This model assumes that any temporal or spatial variation in the the atmospheric drag acceleration can be neglected, and the overall impact of the atmospheric drag acceleration can be well-represented through its average value. For the time-scale of maneuvers considered in this work (~10 hours), such an approximation is reasonable as the period of spatial variations in the atmospheric drag acceleration in low-Earth orbit (e.g., from the day-night cycle as experienced by the spacecraft) will be much faster than the maneuver length, and the maneuver length is too short for appreciable temporal change (e.g., from solar activity) in the atmospheric density.

Throughout the spacecraft's trajectory, it is assumed that measurements are collected of the spacecraft's deviation in radial and along-track position relative to a known reference trajectory. This reference trajectory corresponds to a simulation of the spacecraft's trajectory when $\boldsymbol{\phi} = \mathbf{0}$. As such, the measurement vector is given by

$$\boldsymbol{y} = \begin{bmatrix} \Delta r(\tau_1) & \dots & \Delta r(\tau_m) & \Delta s(\tau_1) & \dots & \Delta s(\tau_m) \end{bmatrix}^T \tag{2}$$

where $\boldsymbol{\tau} = \{\tau_1, \dots, \tau_m\}$ is a set of m chronologically-ordered measurement times. Again, deviations in the cross-track direction for both the position and velocity are neglected, as their sensitivities to an along-track acceleration are zero. Both the parameter and measurement vectors have corresponding covariance matrices of $[\Sigma_{\boldsymbol{\phi}}]$ and $[\Sigma_{\boldsymbol{y}}]$ respectively.

It has been shown, in Ref. [4], that the parameter and measurement vectors are approximately linearly related as

$$\boldsymbol{y} \approx [H(\boldsymbol{\tau})]\boldsymbol{\phi} \tag{3}$$

where each element of the measurement matrix, $[H(\boldsymbol{\tau})]$, contains the sensitivity for deviations in the spacecraft's radial and along-track position with respect to the initial position and velocity, the magnitude of the atmospheric drag acceleration, and the magnitude of each segment of the propulsive acceleration. For each of the acceleration magnitudes, whether atmospheric drag or propulsive, the sensitivity of the radial position with respect to the acceleration magnitude is approximately

$$\frac{\partial}{\partial a}\Delta r(t) \approx \begin{cases} 0 & t < t_{\text{start}} \\ \frac{2r_0}{v_{s,0}}(t - t_{\text{start}}) & t_{\text{start}} \leq t < t_{\text{end}} \\ \frac{2r_0}{v_{s,0}}(t_{\text{end}} - t_{\text{start}}) & t_{\text{end}} < t \end{cases} \tag{4}$$

where t_{start} and t_{end} are the start and end times of the time interval where the acceleration segment is active. For atmospheric drag, t_{start} and t_{end} correspond to the start and end time of the entire maneuver period while for the propulsive acceleration t_{start} and t_{end} correspond to the start and end time of each segment. The sensitivity of the

along-track position with respect to the acceleration magnitude is approximately

$$\frac{\partial}{\partial a}\Delta s(t) \approx \begin{cases} 0 & t < t_{\text{start}} \\ -\frac{3}{2}(t - t_{\text{start}})^2 & t_{\text{start}} \leq t < t_{\text{end}} \\ -3(t_{\text{end}} - t_{\text{start}})\left[(t - t_{\text{start}}) - \frac{1}{2}(t_{\text{end}} - t_{\text{start}})\right] & t_{\text{end}} < t \end{cases} \tag{5}$$

Both Eq. 4 and 5 are derived in Ref. [4]. The sensitivities of the spacecraft's radial and along-track positions with respect to the initial position and velocity deviations in the local-vertical, local-horizontal frame are directly given by linear orbit theory [24].

Given the analytical approximation for the measurement matrix, the covariance of the parameter vector conditioned on a given measurement vector can be calculated from

$$[\Sigma^+_{\boldsymbol{\phi}}(\boldsymbol{\tau})] = \left([\Sigma^-_{\boldsymbol{\phi}}]^{-1} + [H(\boldsymbol{\tau})]^T [\Sigma_{\mathbf{y}}]^{-1} [H(\boldsymbol{\tau})]\right)^{-1} \tag{6}$$

where $[\Sigma^-_{\boldsymbol{\phi}}]$ represents a prior parameter covariance matrix, allowing for the inclusion of prior knowledge in the calculation. The measurement matrix, $[H(\boldsymbol{\tau})]$, and posterior covariance of the parameter vector, $[\Sigma^+_{\boldsymbol{\phi}}(\boldsymbol{\tau})]$, can both be rapidly (i.e. without any numerical simulation) calculated given a choice of measurement times, $\boldsymbol{\tau}$. Define $[\Sigma^+_{a_{1:n}}(\boldsymbol{\tau})]$ to correspond to the lower-right $n \times n$ block of $[\Sigma^+_{\boldsymbol{\phi}}(\boldsymbol{\tau})]$ which defines the covariance matrix for the propulsive accelerations. Since $[\Sigma^+_{a_{1:n}}(\boldsymbol{\tau})]$ depends on the choice of measurement times, it suggests that given a fixed number of measurements, m, there is a way to select the set of measurement times, $\boldsymbol{\tau}$, such that the posterior uncertainty in the propulsive accelerations is minimized. In particular, we can solve the optimization problem

$$\begin{aligned} \min_{\boldsymbol{\tau}} \quad & \text{trace}\left([\Sigma^+_{a_{1:n}}(\boldsymbol{\tau})]\right) \\ \text{subject to} \quad & \tau_{i+1} - \tau_i \geq \Delta t_{\min} \quad \forall i \in \{1, \ldots, m-1\} \\ \text{and} \quad & \tau_m \leq T \end{aligned} \tag{7}$$

where $\Delta t_{\min}$ defines a minimum time interval between measurements, and T defines the overall time of the measurement period. In this work, a local optimal for $\boldsymbol{\tau}$ is solved for using MATLAB's `fmincon` function starting from an initial guess for $\boldsymbol{\tau}$ which evenly distributes the measurement times across the measurement period.

III. Implementation

Implementation of the measurement timing optimization can occur early in the mission design process. The only information that is required is the initial orbital radius of the spacecraft, the start and end times of each segment of the

piecewise-constant representation of the propulsive acceleration, and the prior parameter and measurement covariance matrices. Given this information, the posterior parameter covariance matrix can be calculated from Eq. 6, which in turn allows the measurement time vector to be optimized such that the posterior uncertainty in the propulsive accelerations is minimized. Note that the sensitivity approximations for the spacecraft's radial and along-track positions in Eqs. 4 and 5 do not depend on the actual acceleration value. As such, the optimization of the measurement time vector can be carried out before the propulsive accelerations are known, and the resulting posterior uncertainty in the propulsive accelerations will be independent of the actual acceleration values.

One key aspect for inference of the propulsive accelerations that does need to be considered in the mission design process is the ability to distinguish between the atmospheric drag and propulsive accelerations. If the propulsive acceleration is uncertain throughout the entire maneuver period, then the parameter vector will be unobservable. In particular, it will be impossible to tell the difference between cases where all of the propulsive acceleration magnitudes are biased by some Δa and the atmospheric drag acceleration is biased by $-\Delta a$ for different Δa as they would all produce the same spacecraft trajectory. As such, it is required that there be some portion of the measurement period where the propulsive acceleration is known exactly. The only time the propulsive acceleration is known exactly is if the propulsion system is known to be inactive, and the only along-track acceleration acting on the spacecraft is the atmospheric drag acceleration. In this case, the atmospheric drag acceleration can be determined based on the portion of the measurement period where the propulsion system is known to be inactive, which in turn allows the propulsive acceleration in the other portions of the measurement period to be resolved.

IV. Examples

This section demonstrates the measurement timing optimization for three different cases: a case where the propulsive acceleration only has a single segment, $n = 1$; a case where the propulsive acceleration has three segments, $n = 3$; and a case where the propulsive acceleration has three segments, but the optimization only minimizes the posterior variance of one of the segments. In all cases, the maneuvers are designed in the same manner where the maneuver period is broken into $n + 1$ evenly-distributed segments. During the first n segments, the propulsion system is active with each segment corresponding to one of the segments in the piecewise-constant representation of the propulsive acceleration. During the final segment, the propulsion system is assumed to be inactive such that the propulsive acceleration is known to be zero and the atmospheric drag acceleration can be determined. For the case where the propulsive acceleration has a single segment, the maneuver period is 10 hours such that the propulsive acceleration acts over the first five hours. For the cases where the propulsive acceleration has three segments, the maneuver period is 16 hours such that each segment of the piecewise-constant representation of the propulsive acceleration acts over four hours.

In all cases, the spacecraft is assumed to initially be in a 425 km altitude circular orbit around Earth with inclination of 52 degrees for the case where the propulsive acceleration has one segment and 90 degrees for the cases where the

propulsive acceleration has three segments. The magnitude of the average atmospheric drag acceleration is assumed to be 5 μm/s^2, and the magnitudes of any propulsive accelerations are randomly selected on the range 0–25 μm/s^2. The orbit inclination is only relevant for numerical comparison of the optimization results in order to ensure that there are no impacts of different inclinations on the inference process, and does not impact any aspect of the approach in Section II. Similarly, the posterior parameter covariance, $[\Sigma^+_{\boldsymbol{\phi}}(\boldsymbol{\tau})]$, is independent of the actual acceleration magnitudes as neither Eq. 4 nor Eq. 5 depends on the acceleration magnitude. Therefore, the results of this example are applicable to other atmospheric drag or propulsive accelerations for the same orbit altitude and maneuver segment timings.

For the purposes of this work, the prior distributions for each of the parameters are assumed to be independent such that the prior parameter covariance matrix is

$$[\Sigma^-_{\boldsymbol{\phi}}] = \text{diag}\left(\left[\sigma_p^2\mathbf{1}_{1\times 2} \quad \sigma_v^2\mathbf{1}_{1\times 2} \quad \sigma_a^2\mathbf{1}_{1\times n+1}\right]\right) \tag{8}$$

where $\sigma_p = 100/3$ m, $\sigma_v = 1/3$ m/s, $\sigma_a = 25/3$ μm/s^2, and $\mathbf{1}_{1\times q}$ is a $1\times q$ vector of ones. A prior parameter covariance is not required, and in the case of no prior information the inverse of the prior parameter covariance in Eq. 6 can be set to $[\Sigma^-_{\boldsymbol{\phi}}]^{-1} = [0_{n+5}]$ where $[0_{n+5}]$ is an $(n+5)\times(n+5)$ zero matrix. The distributions for the uncertainty in each measurement are assumed to be independent and identically distributed such that the measurement covariance is

$$[\Sigma_{\boldsymbol{y}}] = \sigma_p^2[I_{2m}] \tag{9}$$

where $[I_{2m}]$ is a $2m\times 2m$ identity matrix. In all cases there are 50 measurement locations, $m = 50$. For the case where the propulsive acceleration has one segment, the minimum measurement interval is five minutes, $\Delta t_{\text{min}} = 5$ min. For the cases where the propulsive acceleration has three segments, the minimum measurement interval is 10 minutes.

A. Single Acceleration

Figure 1 shows a comparison between an analytically-calculated and numerically-estimated along-track measurement pseudoinverse for the case where the propulsive acceleration only has a single segment, $n = 1$. Markers indicate measurement times while shading indicates the interval of time where each acceleration is active. The along-track measurement pseudoinverse is defined as the elements of the pseudoinverse of the measurement matrix

$$[H(\boldsymbol{\tau})]^+ = \left([H(\boldsymbol{\tau})]^T[H(\boldsymbol{\tau})]\right)^{-1}[H(\boldsymbol{\tau})]^T \tag{10}$$

which relate changes in the along-track position of the spacecraft to changes in each acceleration; for the atmospheric drag acceleration they correspond to the second half of the fifth row of $[H(\boldsymbol{\tau})]^+$ while for segment i of the propulsive acceleration they correspond to the second half of row $i+5$ of $[H(\boldsymbol{\tau})]^+$. In Figure 1, these elements are shown versus

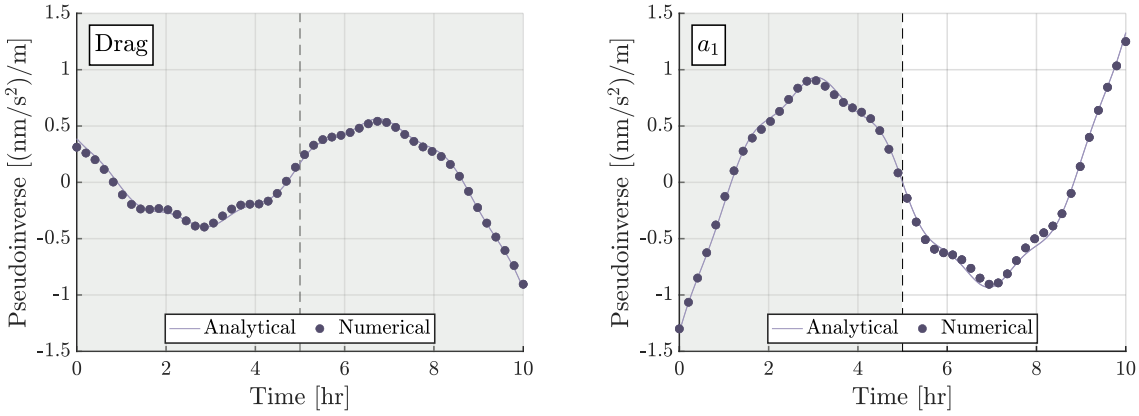

Fig. 1 Comparison between the analytically-calculated and numerically-estimated along-track measurement pseudoinverse for a single propulsive acceleration.

the corresponding time of each measurement. The analytical and numerical results agree quite closely.

Since the analytically-calculated and numerically-estimated along-track measurement pseudoinverse agree quite closely, the estimate of the posterior parameter covariance matrix for a given measurement time vector in Eq. 6 is assumed to be accurate. Figure 2 shows the analytically-calculated along-track measurement pseudoinverse both before and after carrying out the optimization in Eq. 7, where the initial guess for the measurement time vector was to evenly distribute the measurements over the entire measurement period (i.e. have a constant measurement interval). Markers indicate measurement times while shading indicates the interval of time where each acceleration is active. The optimization quite clearly clusters measurements near local extrema in the along-track measurement pseudoinverse for the propulsive acceleration, a_1. This intuitively makes sense as from Eqs. 4 and 5 the sensitivity of the along-track position with respect to any along-track acceleration is quadratic in time whereas the sensitivity of the radial position is only linear in time. Therefore, changes in the along-track position provide more information about any along-track accelerations acting on the spacecraft, except for measurement times within approximately 1/5 of the period of the spacecraft's initial orbit. The local extrema in the along-track measurement pseudoinverse for the propulsive acceleration also closely correspond to local extrema in the along-track measurement pseudoinverse for the atmospheric drag acceleration. Again this makes intuitive sense as uncertainty in the atmospheric drag acceleration needs to be reduced in order to minimize the uncertainty in the propulsive acceleration.

Table 1 shows the results of the optimization on the standard deviations for the atmospheric drag and propulsive accelerations. The posterior standard deviations are shown both from an analytical calculation using Eq. 6 and from full numerical inference using an ensemble Kalman update approach [19]. The standard deviation for both accelerations decreases by approximately 20% when using the optimized measurement time vector relative to a constant measurement interval. The posterior standard deviations also agree quite well between the analytical prediction and numerical inference, further verifying the results of the optimization approach in Section II. The data of Table 1 demonstrate

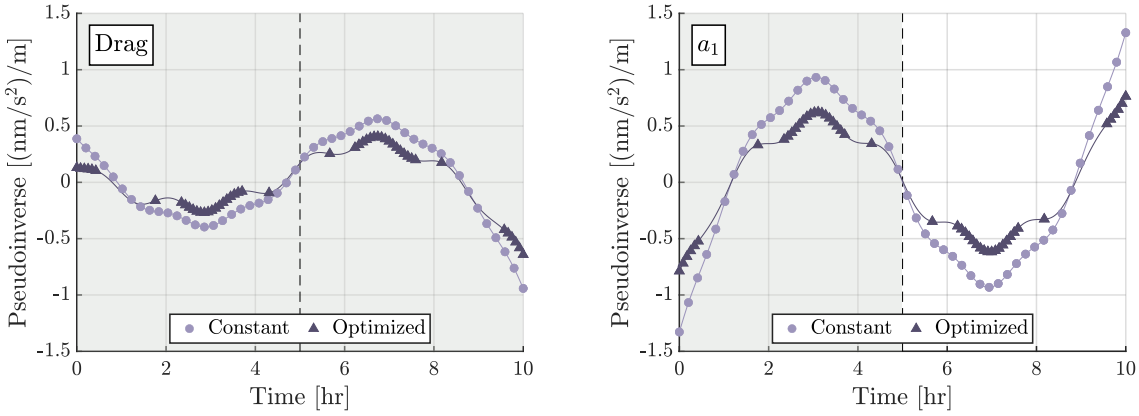

Fig. 2 Comparison between the constant and optimized measurement timings in the analytically-calculated along-track measurement pseudoinverse for a single propulsive acceleration.

Table 1 Impact of optimizing the measurement timing on the posterior standard deviation of the different acceleration magnitudes for a single propulsive acceleration.

	Analytical Prediction [μm/s^2]			Numerical Inference [μm/s^2]		
Acceleration	Constant	Optimized	Change [%]	Constant	Optimized	Change [%]
Drag	0.0873	0.0711	-18.6	0.0855	0.0699	-18.2
a_1	0.1597	0.1273	-20.3	0.1549	0.1241	-19.8

that purely through optimization of the measurement timings, a significant (20%) reduction in the posterior standard deviation of the propulsive acceleration estimate can be achieved.

B. Multiple Accelerations

In some situations, it may be required to infer multiple different propulsive accelerations such as when attempting to reconstruct long-duration propulsive maneuvers with a segmented approach [4]. The optimization approach of Section II can be applied to an arbitrary number of propulsive acceleration segments. Here it is demonstrated for the case that the propulsive acceleration has three segments, $n = 3$. As in the single-segment case, a comparison between the analytically-calculated and numerically-estimated along-track measurement pseudoinverse is shown in Figure 3. Markers indicate measurement times while shading indicates the interval of time where each acceleration is active. Again, the analytical and numerical results agree quite closely. These results demonstrate that the estimate of the posterior parameter covariance matrix for a given measurement time vector in Eq. 6 can be assumed to be accurate when multiple propulsive acceleration segments are used.

Figure 4 shows the analytically-calculated along-track measurement pseudoinverse both before and after carrying out the optimization in Eq. 7, where the initial guess for the measurement time vector again used a constant measurement interval such that the measurements were evenly distributed over the measurement period. Markers indicate measurement times while shading indicates the interval of time where each acceleration is active. The cost function in Eq. 7 aims

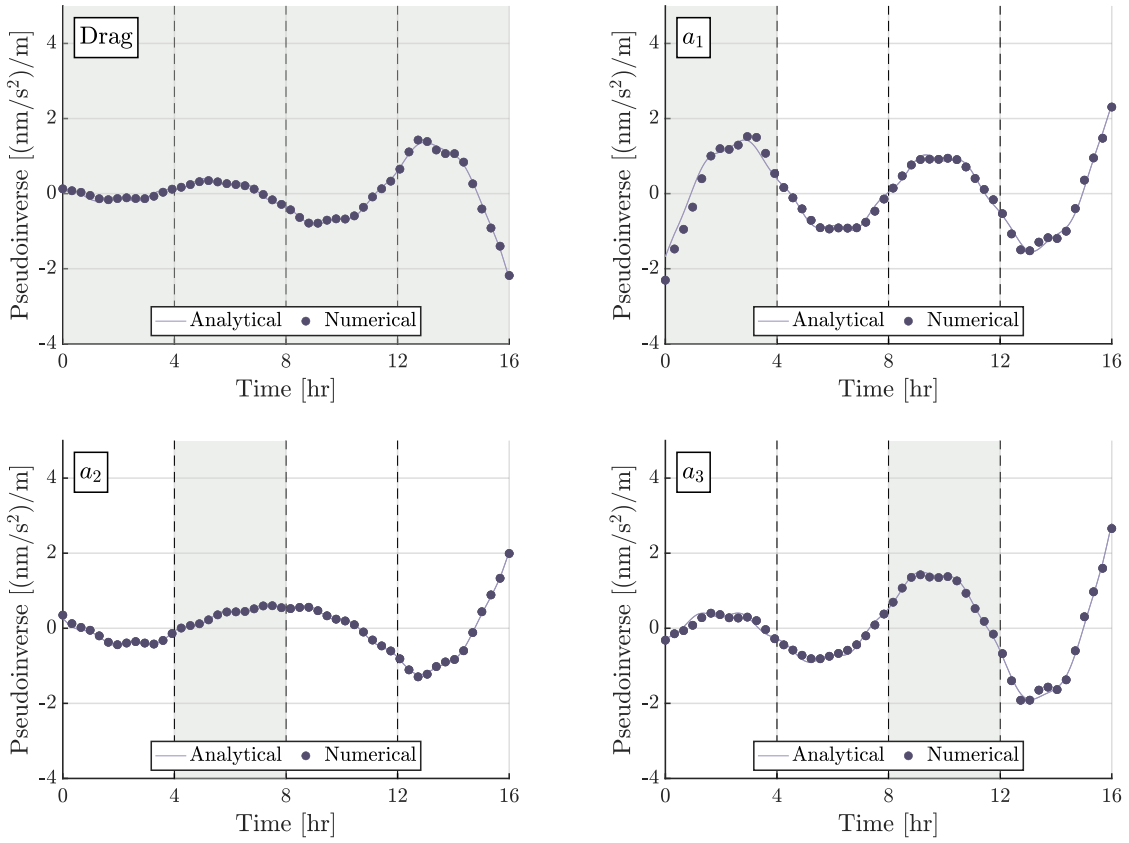

Fig. 3 Comparison between the analytically-calculated and numerically-estimated along-track measurement pseudoinverse for multiple propulsive accelerations.

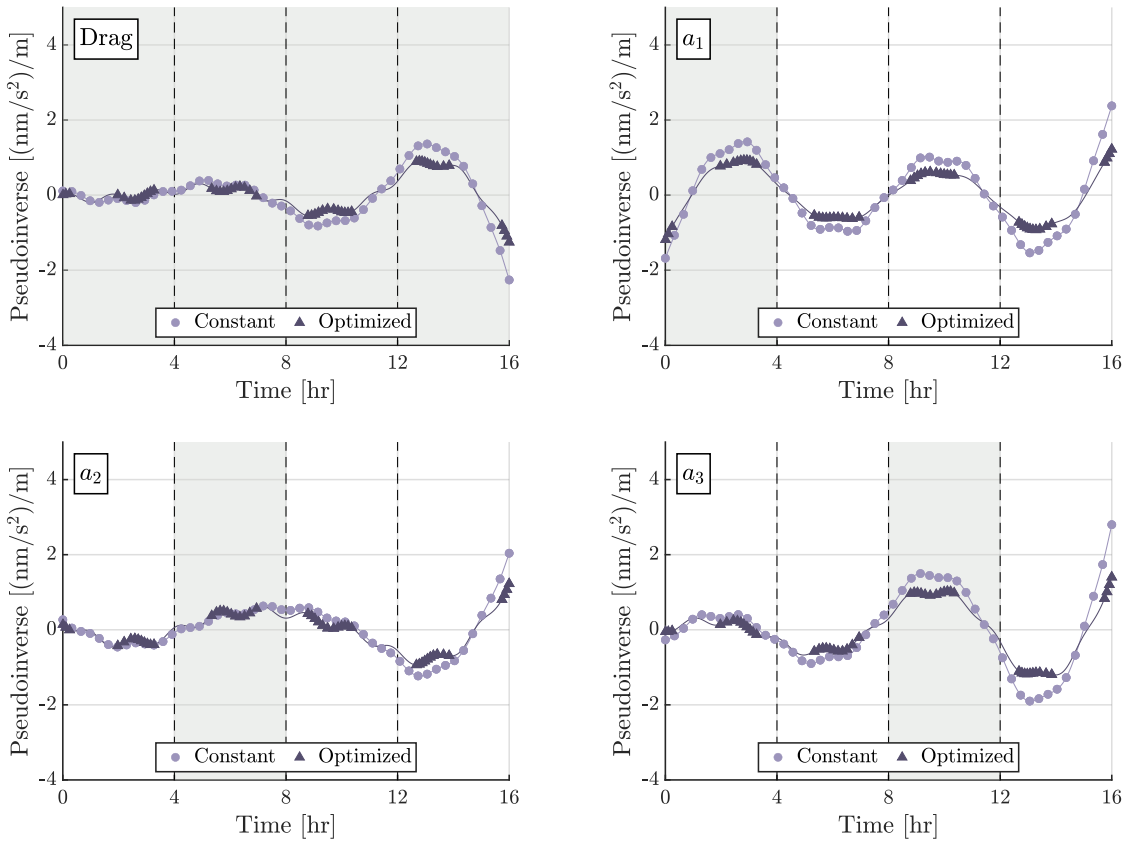

Fig. 4 Comparison between the constant and optimized measurement timings in the analytically-calculated along-track measurement pseudoinverse for multiple propulsive accelerations.

to minimize the sum of posterior variances for the propulsive accelerations. As such, the optimized measurement timings are again concentrated near local extrema in the along-track measurement pseudoinverse for the propulsive accelerations: a_1, a_2, and a_3. As in the case with a single propulsive acceleration segment, the local extrema in the along-track measurement pseudoinverse for each of the propulsive accelerations closely correspond to local extrema in the along-track measurement pseudoinverse for the atmospheric drag acceleration. Table 2 shows the results of the optimization on the standard deviations for the atmospheric drag and propulsive accelerations. As in the single propulsive segment case, the standard deviation in all accelerations decreases by approximately 20% when using the optimized measurement time vector relative to a constant measurement interval. The posterior standard deviations also continue to agree quite well between the analytical prediction and numerical inference. Again, purely through optimization of the measurement timings, significant (20%) reduction in the posterior standard deviation of the propulsive acceleration estimates can be achieved.

Table 2 Impact of optimizing the measurement timing on the posterior standard deviation of the different acceleration magnitudes for multiple propulsive accelerations.

	Analytical Prediction [μm/s^2]			Numerical Inference [μm/s^2]		
Acceleration	Constant	Optimized	Change [%]	Constant	Optimized	Change [%]
Drag	0.1630	0.1270	-22.1	0.1596	0.1257	-21.2
a_1	0.2393	0.1885	-21.2	0.2337	0.1869	-20.0
a_2	0.1523	0.1273	-16.4	0.1500	0.1259	-16.1
a_3	0.2442	0.1935	-20.8	0.2364	0.1882	-20.4

C. Multiple Accelerations, Optimization of a Single Acceleration

As a final case, we can consider a similar scenario to Section IV.B, but where the posterior standard deviation of only a single segment of the propulsive acceleration is minimized—the only difference in the optimization for this case relative to that of Section IV.B is that the cost function of Eq. 7 is modified to consider the diagonal element of $[\Sigma^{+}_{\phi}(\boldsymbol{\tau})]$ corresponding to the marginal variance of only one of the propulsive acceleration magnitudes. Figure 5 shows the analytically-calculated along-track measurement pseudoinverse both before and after carrying out the optimization in Eq. 7, but with the cost function modified to only minimize the posterior marginal variance of the propulsive acceleration for the second segment, a_2. Markers indicate measurement times while shading indicates the interval of time where each acceleration is active. As before, the initial guess for the measurement time vector used a constant measurement interval such that the measurements were evenly distributed over the measurement period. In this case, the optimized measurement time vector is similar to the single-segment case where measurements are concentrated near local extrema in the along-track measurement pseudoinverse for acceleration a_2 with little regard for the other acceleration segments.

Table 3 shows the results of this modified optimization on the standard deviations for the atmospheric drag and propulsive accelerations. Compared to the results of Section IV.B, the posterior standard deviation of acceleration a_2 is reduced by a further 8% for a total reduction of approximately 24%—or 25% if considering the results of the numerical inference—when using the optimized measurement time vector relative to a constant measurement interval. The posterior standard deviations of the atmospheric drag acceleration and propulsive accelerations a_1 and a_3 only see modest reductions of approximately 10%, 2%, and 9% respectively. As a result, slight improvements in the optimized posterior standard deviation for the propulsive acceleration of a single segment can be achieved for the cost of notable deterioration in the standard deviation of the other segments. In particular, when all three propulsive acceleration segments were optimized together, in Section IV.B, the change in the posterior standard deviation of acceleration a_1 due to optimization of the measurement time vector was approximately 21% whereas in this case it was only 2%.

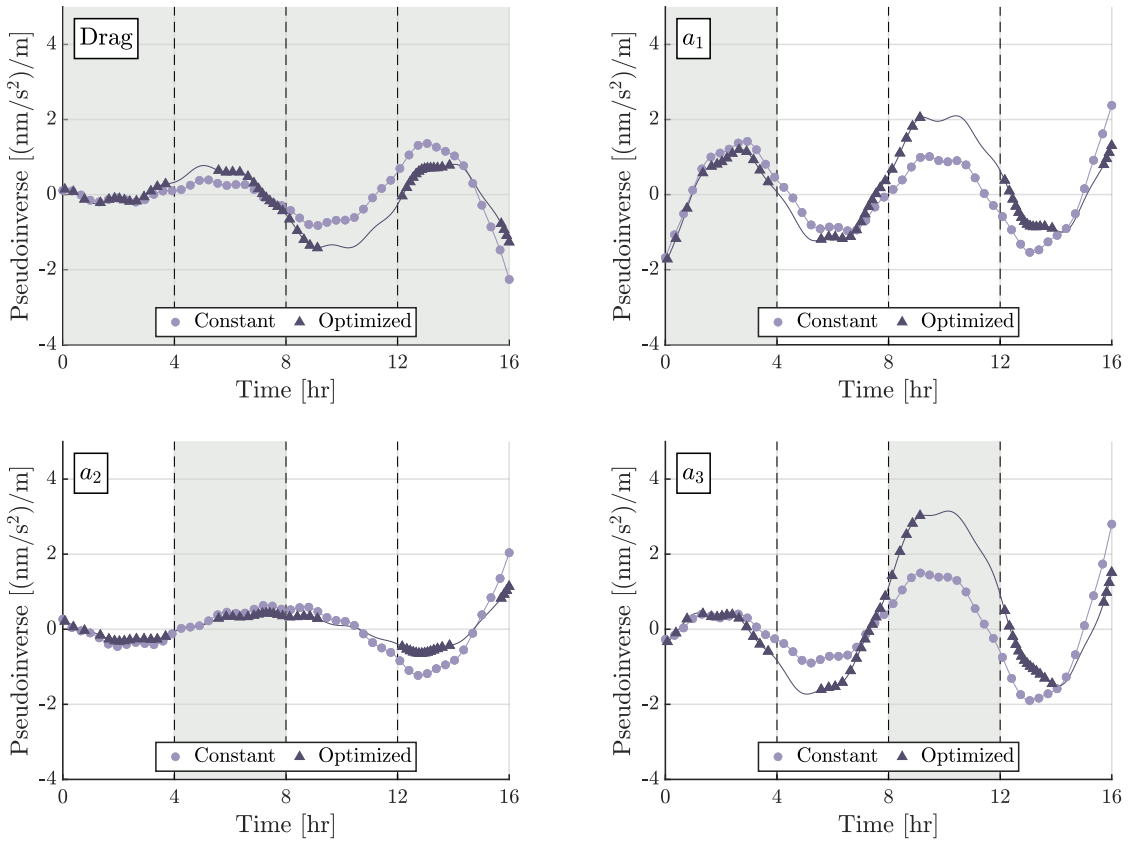

Fig. 5 Comparison between the constant and optimized measurement timings in the analytically-calculated along-track measurement pseudoinverse, but only the posterior variance of acceleration a_2 is optimized.

Table 3 Impact of optimizing the measurement timing on the posterior standard deviation of the different acceleration magnitudes for multiple propulsive accelerations, but only acceleration a_2 is optimized.

	Analytical Prediction [μm/s^2]			Numerical Inference [μm/s^2]		
Acceleration	Constant	Optimized	Change [%]	Constant	Optimized	Change [%]
Drag	0.1630	0.1468	-9.9	0.1608	0.1439	-10.5
a_1	0.2393	0.2344	-2.0	0.2333	0.2280	-2.3
a_2	0.1523	0.1152	-24.3	0.1522	0.1141	-25.0
a_3	0.2442	0.2662	-9.0	0.2375	0.2567	-8.0

V. Conclusion

This paper demonstrates that for the problem of on-orbit inference of along-track propulsive accelerations, the timing of a fixed number of measurements can be optimized—without the use of numerical simulation—in order to achieve notable reductions in the posterior uncertainty of the propulsive acceleration estimates. In the example cases considered here, reductions in the posterior standard deviation of approximately 20% were achieved, purely due to the optimization of the measurement timing. The primary benefit of this work is for data-limited scenarios including: limitations on the number of measurements that can be taken due constraints in the sensor system; limitations on the number of measurements that can be transmitted to Earth due to constraints in the communications system; and limitations on the number of measurements that can be processed due to computational constraints either on the spacecraft or on Earth. In all of these scenarios, the results of this work provide a method to optimize the timing of spacecraft position measurements in order to minimize the posterior uncertainty in the propulsive accelerations.

References

[1] Kerslake, W. R., Goldman, R. G., and Nieberding, W. C., "SERT II: Mission, Thruster Performance, and In-Flight Thrust Measurements," *Journal of Spacecraft and Rockets*, Vol. 8, No. 3, 1971, pp. 213–224. https://doi.org/10.2514/3.30250.

[2] Rafalskyi, D., Martínez Martínez, J., Habl, L., Zorzoli Rossi, E., Proynov, P., Boré, A., Baret, T., Poyet, A., Lafleur, T., Dundin, S., and Aanesland, A., "In-Orbit Demonstration of an Iodine Electric Propulsion System," *Nature*, Vol. 599, 2021, pp. 411–415. https://doi.org/10.1038/s41586-021-04015-y.

[3] Krejci, D. and Reissner, A., "Large Number System Integration Aspects: On Orbit Data and Lessons Learnt from Launching 144 FEEP Propulsion Systems," *Journal of Electric Propulsion*, Vol. 1, No. 30, 2022. https://doi.org/10.1007/s44205-022-00020-z.

[4] Jia-Richards, O., "Segmented Reconstruction of Low-Acceleration Orbital Maneuvers," *Journal of Guidance, Control, and Dynamics*, Vol. 46, No. 12, 2023, pp. 2290–2299. https://doi.org/10.2514/1.G007548.

[5] Goff, G. M., Black, J. T., and Beck, J. A., "Orbit Estimation of a Continuously Thrusting Spacecraft Using Variable Dimension Filters," *Journal of Guidance, Control, and Dynamics*, Vol. 38, No. 12, 2015, pp. 2407–2420. https://doi.org/10.2514/1.G001091.

[6] Kaderali, S. and Misra, A., "Detection and Characterisation of Unknown Maneuvers in Spacecraft," *Acta Astronautica*, Vol. 205, 2023, pp. 310–318. https://doi.org/10.1016/j.actaastro.2023.01.018.

[7] Porcelli, L., Pastor, A., Cano, A., Escribano, G., Sanjurjo-Rivo, M., Escobar, D., and Di Lizia, P., "Satellite Maneuver Detection and Estimation with Radar Survey Observations," *Acta Astronautica*, Vol. 201, 2022, pp. 274–287. https://doi.org/10.1016/j.actaastro.2022.08.021.

[8] Kelecy, T. and Jah, M., "Detection and Orbit Determination of a Satellite Executing Low Thrust Maneuvers," *Acta Astronautica*, Vol. 66, 2010, pp. 798–809. https://doi.org/10.1016/j.actaastro.2009.08.029.

[9] Lemmens, S. and Krag, H., "Two-Line-Element-Based Maneuver Detection Methods for Satellites in Low Earth Orbit," *Journal of Guidance, Control, and Dynamics*, Vol. 37, No. 3, 2014, pp. 860–868. https://doi.org/10.2514/1.61300.

[10] Li, T., Li, K., and Chen, L., "Maneuver Detection Method Based on Probability Distribution Fitting of the Prediction Error," *Journal of Spacecraft and Rockets*, Vol. 56, No. 4, 2019, pp. 1114–1120. https://doi.org/10.2514/1.A34301.

[11] Goff, G. M., Black, J. T., and Beck, J. A., "Tracking Maneuvering Spacecraft with Filter-Through Approaches using Interacting Multiple Models," *Acta Astronautica*, Vol. 114, 2015, pp. 152–163. https://doi.org/10.1016/j.actaastro.2015.05.009.

[12] Lee, S., Lee, J., and Hwang, I., "Maneuvering Spacecraft Tracking via State-Dependent Adaptive Estimation," *Journal of Guidance, Control, and Dynamics*, Vol. 39, No. 9, 2016, pp. 2034–2043. https://doi.org/10.2514/1.G001567.

[13] Holzinger, M. J., Scheeres, D. J., and Alfriend, K. T., "Object Correlation, Maneuver Detection, and Characterization Using Control-Distance Metrics," *Journal of Guidance, Control, and Dynamics*, Vol. 35, No. 4, 2012, pp. 1312–1325. https://doi.org/10.2514/1.53245.

[14] Jaunzemis, A. D., Mathew, M. V., and Holzinger, M. J., "Control Cost and Mahalanobis Distance Binary Hypothesis Testing for Spacecraft Maneuver Detection," *Journal of Guidance, Control, and Dynamics*, Vol. 39, No. 9, 2016, pp. 2058–2072. https://doi.org/10.2514/1.G001616.

[15] Serra, R., Yanez, C., and Frueh, C., "Tracklet-to-Orbit Association for Maneuvering Space Objects using Optimal Control Theory," *Acta Astronautica*, Vol. 181, 2021, pp. 271–281. https://doi.org/10.1016/j.actaastro.2021.01.026.

[16] Ko, H. and Scheeres, D. J., "Tracking Maneuvering Satellite Using Thrust-Fourier-Coefficient Event Representation," *Journal of Guidance, Control, and Dynamics*, Vol. 39, No. 11, 2016, pp. 2554–2562. https://doi.org/10.2514/1.G000353.

[17] Zhou, X., Qin, T., and Meng, L., "Maneuvering Spacecraft Orbit Determination Using Polynomial Representation," *Aerospace*, Vol. 9, No. 5, 2022, p. 257. https://doi.org/10.3390/aerospace9050257.

[18] Craft, K. J., Hecht, G. R., Darling, J. E., and Pernicka, H. J., "Development, Verification, and Analysis of a Small Satellite Thrust Determination Filter," *Journal of Spacecraft and Rockets*, Vol. 59, No. 2, 2022, pp. 360–374. https://doi.org/10.2514/1.A35147.

[19] Jia-Richards, O., Marzouk, Y. M., and Lozano, P. C., "A Method for Direct In-Space Thrust Estimation from Low-Acceleration Orbital Maneuvers," *Journal of Electric Propulsion*, Vol. 2, No. 19, 2023. https://doi.org/10.1007/s44205-023-00054-x.

[20] Jia-Richards, O. and Lafleur, T., "Iodine Electric Propulsion System Thrust Validation: From Numerical Modeling to In-Space Testing," *Journal of Propulsion and Power*, Vol. 39, No. 6, 2023, pp. 896–904. https://doi.org/10.2514/1.B39198.

[21] Frueh, C., Fielder, H., and Herzog, J., "Heuristic and Optimized Sensor Tasking Observation Strategies with Exemplification for Geosynchronous Objects," *Journal of Guidance, Control, and Dynamics*, Vol. 41, No. 5, 2018, pp. 1036–1048. https://doi.org/10.2514/1.G003123.

[22] Little, B. D. and Frueh, C. E., "Space Situational Awareness Sensor Tasking: Comparison of Machine Learning with Classical Optimization Methods," *Journal of Guidance, Control, and Dynamics*, Vol. 43, No. 2, 2020, pp. 262–273. https://doi.org/10.2514/1.G004279.

[23] Siew, P. M., Jang, D., Roberts, T. G., and Linares, R., "Space-Based Sensor Tasking Using Deep Reinforcement Learning," *Journal of the Astronautical Sciences*, Vol. 69, 2022, pp. 1855–1892. https://doi.org/10.1007/s40295-022-00354-8.

[24] Clohessy, W. H. and Wiltshire, R. S., "Terminal Guidance System for Satellite Rendezvous," *Journal of the Aerospace Sciences*, Vol. 27, No. 9, 1960, pp. 653–658. https://doi.org/10.2514/8.8704.